Carbohydrate Polymers 117 (2015) 746–752

Contents lists available at ScienceDirect

Carbohydrate Polymers

journal homepage: www.elsevier.com/locate/carbpol

Interphase vs confinement in starch-clay bionanocomposites

Gildas Coativy[a,b,c], Chloé Chevigny[b,c], Agnès Rolland-Sabaté[b,c], Eric Leroy[a,c,*], Denis Lourdin[b,c]

[a] LUNAM Université, CNRS, GEPEA, UMR 6144, CRTT, 37, Boulevard de l'Université, 44606 St Nazaire Cedex, France
[b] UR1268 Biopolymères Interactions Assemblages, INRA, F-44300 Nantes, France
[c] Structure Fédérative IBSM, INRA Nantes-Angers, Rue de la Géraudière, BP 71627, 44316 Nantes Cedex 3. France

ARTICLE INFO

Article history:
Received 28 February 2014
Received in revised form 5 September 2014
Accepted 17 October 2014
Available online 30 October 2014

Keywords:
Starch
Clay
Nanocomposite
Confinement
Macromolecular dynamics

ABSTRACT

Starch-clay bionanocomposites containing 1–10% of natural montmorillonite were elaborated by melt processing in the presence of water. A complex macromolecular dynamics behavior was observed: depending on the clay content, an increase of the glass transition temperature and/or the presence of two overlapped α relaxation peaks were detected. Thanks to a model allowing the prediction of the average interparticle distance, and its comparison with the average size of starch macromolecules, it was possible to associate these phenomena to different populations of macromolecules. In particular, it seems that for high clay content (10%), the slowdown of segmental relaxation due to confinement of the starch macromolecules between the clay tactoïds is the predominant phenomenon. While for lower clay contents (3–5%), a significant modification of chain relaxation seems to occur, due to the formation of an interphase by the starch macromolecules in the vicinity of clay nanoparticles coexisting with the bulk polymer.

1. Introduction

Among the characteristics of polymer nanocomposites that distinguish these materials from "classic" filled polymer systems, the fact that both the size of rigid nanoparticles inclusions and the interparticle distances can become comparable to the size and relaxation volume of polymer chains (Giannelis, 1998; Kalfus & Jancar, 2008; Vaia & Wagner, 2004) are often seen as the factor most likely to affect their thermo-mechanical properties (Jancar et al., 2010; Kalfus & Jancar, 2008). A quantitative equivalence has been even drawn between polymer nanocomposites and thin polymer films (Bansal et al., 2005; Rittigstein, Priestley, Broadbelt, & Torkelson, 2007).

Actually, two kinds of phenomena affecting the macromolecular dynamics have been reported so far. The most frequently reported phenomenon is a slowdown of the segmental relaxation of macromolecules that are confined between nanoparticles or which are in their vicinity. This results either in an increase or a decrease of the glass transition temperature depending on the affinity between the polymer and the surface of nanoparticles (Fotadiou et al., 2013; Fragiadakis, Bokobza, & Pissis, 2011; Rittigstein & Torkelson, 2006; Rittigstein et al., 2007; Vaia, Sauer, Tse, Giannelis, 1997).

Concurrently, the flow relaxation of polymer chains (by diffusion/reptation) can also be modified due to their interactions with the surface of the nanoparticles (Kalfus & Jancar, 2007; Robertson & Rackaitis, 2011). In such a case, thermomechanical relaxations can be observed well above the glass transition temperature of the material (Robertson & Rackaitis, 2011).

These two phenomena will be affected by the ratio between the interparticle distance and the size of the polymer interfacial region (or interphase) responsible for 'communication' between the matrix and filler, which ranges about 2 times the radius of gyration of macromolecules (Vaia & Giannelis, 1997; Vaia & Wagner, 2004). Thus for starch, which tends to present very large radii of gyration of the order of 100 nm (Rolland-Sabate, Guilois, Jaillais, & Colonna, 2011; Wu, Twitt, & Gilbert, 2013), strong modifications of the macromolecular dynamics can be expected in nanocomposites. Consequently, we propose to study a model system composed of starch macromolecules and nanoparticles. For this purpose, sodium montmorillonites were chosen due to their hydrophilic nature favoring their compatibility with starch, while potato starch was chosen due to its very low content of minor components such as proteins and lipids.

* Corresponding author at: LUNAM Université, CNRS, GEPEA, UMR 6144, CRTT, 37, Boulevard de l'Université, 44606 St Nazaire Cedex, France.
Tel.: +33 0 2 40 17 26 60; fax: +33 0 240172618.
E-mail addresses: gildascoativy@gmail.com (G. Coativy), chloe.chevigny@nantes.inra.fr (C. Chevigny), agnes.sabate@nantes.inra.fr (A. Rolland-Sabaté), eric.leroy@univ-nantes.fr (E. Leroy), denis.lourdin@nantes.inra.fr (D. Lourdin).

http://dx.doi.org/10.1016/j.carbpol.2014.10.052
0144-8617/

2. Experimental

2.1. Materials and formulations

Potato starch with an amylose/amylopectin ratio of 23/77 was kindly supplied by Roquette frères (Lestrem, France). Sodium montmorillonites (MMT-Na) were purchased from Sigma–Aldrich. MMT-Na powder consists of aggregates of clay tactoids, in which negative charges monocrystalline platelets of 0.95 nm thickness are stacked, with sodium counter ions between the layers. According to the datasheet of the producer (Nanocor), the MMT-Na has a cation exchange capacity of 1450 μ equ g^{-1}. The individual clay platelets have a density of 2.6 and in-plane dimensions typically ranging from 100 to 130 nm. Such a structure is highly hygroscopic and subject to swelling in presence of water. The interlayer spacing (d_{001}) can be increased from 0.96 nm in the dry state, up to 2 nm when four layers of water are intercalated between the clay platelets of the tactoids (Huang, Bassett, & Wu, 1994). Since this phenomenon results in limited attractive forces between the crystalline layers, it was used to favor exfoliation during melt processing: clays were first equilibrated at a water activity of 0.97, leading to a water content of 30% (wet basis (w.b.)) and to a basal spacing d_{001} = 1.6 nm. In parallel, starch was oven dried at 100 °C during 30 min, resulting in a water content of 8% (w.b.). Starch and MMT powders were then blended in a mortar and then rehydrated until reaching a global water content of 30% (w.b.), the day before extrusion. Such a procedure leads to an intimate mixing of powders before melt processing.

2.2. Melt processing and sample preparation

The hydrated powder mixtures were melt-processed with a 7 cm^3 microcompounder (Minilab, Thermo Haake). It consists in a conical co-rotating twin screw system with a backflow channel, which can be used as a batch mixing reactor given that the material can be recirculated rather than exiting through the die.

The hydrated powder mixtures were introduced in the microcompounder at 95 °C, with a screw speed of 100 rpm, and recirculated during 10 min before being extruded at lower screw speed (10 rpm). The typical weight of the final extruded rods was 2 g (since the rest of the material stayed into the recirculating area), with a rectangular section (4 mm wide and 1 mm thick). Extruded rods were stored at 25 °C and 57% RH (relative humidity) during two weeks before characterization. These storage conditions were long enough to reach the equilibrium water uptake, staying well below the glass transition temperature of the material in order to avoid recrystallization.

2.3. Molar mass and molecular size distributions

High performance size-exclusion chromatography coupled with multi-angle laser light scattering (HPSEC-MALLS) was used to measure the molar mass and the size of the macromolecules solubilized in water. Aqueous solvents are θ solvents for starch macromolecules as their second virial coefficient (A_2) in water is near zero (Roger & Colonna, 1992). So the affinity between the solvent and the macromolecules is neutral.

Measurements were performed on native starch and extruded starch rods. The system was run in an eluent made of water and sodium azide (0.02%) eluent. All methods and equipment used were described in a previous paper (Sankri et al., 2010), except the software used for data treatment, which was ASTRA® software from Wyatt Technology Corporation (USA) (version 6.06). The root mean square weight-average radius of gyration was calculated by using the following equation:

$$\bar{R}^2_{Gw} = \frac{\sum_i c_i R^2_{Gi}}{\sum_i c_i} \quad (1)$$

where R_{Gi} and C_i are the radius of gyration and the concentration of the ith slice of the chromatogram.

2.4. Water and clay contents

The amount of clay in extruded samples was checked by thermogravimetric analysis using a TGA 2050 (TA Instruments, DE). About 10 mg of material were heated with a temperature ramp of 10 °C min^{-1} under nitrogen atmosphere until 950 °C to degrade the organic part and keep the mineral part of the materials. The samples were kept at 950 °C during 20 min. The water content of materials (extruded rods) was assessed by dehydration in an oven at 130 °C during at least 24 h, until an equilibrium constant weight was reached.

2.5. Morphology

Transmission electron microscopy was used to observe the morphology of the bionanocomposites, using an HNAR9000 LaB_6 TEM Microscope (Hitachi), with an accelerating voltage of 300 kV (maximum point to point resolution of 0.18 nm). Samples sections were prepared using a Leica UC7 ultramicrotome equipped with a diamond knife. The ultrathin sections were cut at room temperature and under dry conditions and then transferred onto 300 mesh Cu grids coated with a lacey carbon film.

2.6. Structural characterizations

X-ray diffraction was used to characterize extruded rods. Two-dimensional diffraction diagrams were recorded using a Bruker D8 X-ray diffractometer (Karlsruhe, Germany) equipped with a GADDS detector. The X-ray radiation, Cu Kα1 (λ = 0.15406 nm), produced in a sealed tube at 40 kV and 40 mA, was selected and parallelized using crossed Göbel mirrors and collimated to produce a 500 μm diameter beam. The sample to detector distance was 8.7 cm and the Bragg angles used ranged from 3° to 26° (2θ). The recorded intensity was normalized in order to discard the influence of the variation thickness of the samples and then drawn in function as the angle 2θ to obtain diffracting curves.

The thickness of the tactoids and the average number of stacked clay layers per tactoid may be estimated from the width of the peak associated to the interlayer spacing (d_{001}), using the Scherrer formula (Benetti et al., 2005; Jaboyedoff, Kubler & Thelin, 1999).

$$L = \frac{K \times \lambda}{\Delta 2\theta \times \cos(\theta_0)} \quad (2)$$

where K is a constant (0.89), $\Delta 2\theta$ (rad.) is the width at half maximum of the peak, which diffraction angle at the maximum is $2 \times \theta_0$; and λ is the wavelength (0.15406 nm).

L is the coherence length (nm):

$$L = (N - 1) \times d_{001} \quad (3)$$

where N is the number of layers per tactoid. L is approximately equal to the particle thickness if the tactoids are fully disagglomerated.

2.7. Thermal and thermo-mechanical properties

Differential scanning calorimetry (DSC) and dynamic mechanical thermal analysis (DMTA) were used to evaluate the thermal

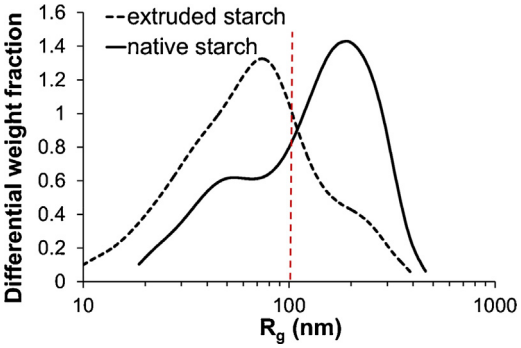

Fig. 1. Differential weight distribution of radius of gyration of native potato starch (straight line) and extruded starch rods (dotted line).

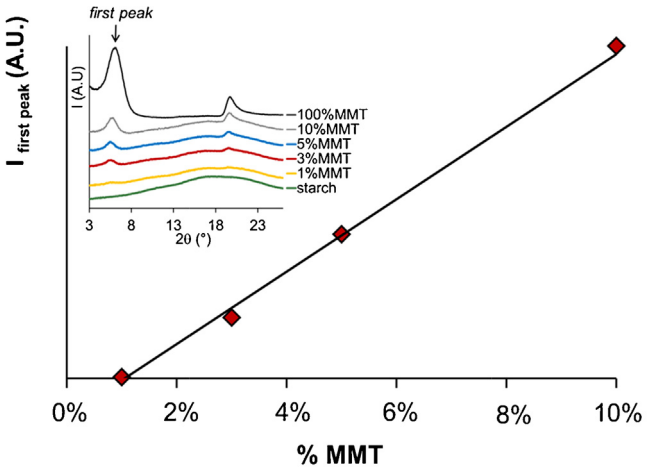

Fig. 2. Tactoid diffracting peak intensity (first peak) vs MMT content.

transitions and the thermo-mechanical behavior of extruded rods, respectively.

A Q100 DSC (T.A. Instruments, New Castle, DE) was used, with inox sealed pans, in order to avoid water loss during tests. Two scan were recorded at 3 °C min^{-1} for each samples from 25 to 95 °C. The glass transition temperature (T_g) was defined as the midpoint of the heat capacity jump.

A MKIV DMTA (Rheometrics Scientific, Piscataway, New Jersey, USA) was used to analyze thermo-mechanical properties. The tensile mode was used at a frequency of 1 Hz, with a temperature ramp from 30 °C to 150 °C at 3 °C min^{-1} and an imposed strain of 0.015%. Sample was coated with hydrophobic grease in order to limit dehydration during the test.

2.8. ^{13}C solid state NMR

NMR experiments were performed on a Bruker DMX-400 spectrometer operating at a ^{13}C frequency of 100.58 MHz and equipped with a double-resonance H/X CP-MAS 4-mm probe for CP-MAS solid state experiments. Experiments were carried at ambient temperature (294 K). Contact time was 1.5 ms. A typical number of 1500 scans was acquired for each spectrum. Chemical shifts were calibrated with external glycin, assigning the carbonyl carbon at 176.03 ppm.

3. Results

3.1. Structural characterization

3.1.1. Influence of processing on molar mass and molecular size distribution

Measurements were conducted on water solubilized starch and extruded starch rods without clays. The weight-average molar mass after extrusion was $\bar{M}_w$ is 0.45×10^8 g mol^{-1}. In comparison, $\bar{M}_w$ is 1.33×10^8 g mol^{-1} for native potato starch. Such a decrease in $\bar{M}_w$ is similar to that observed in literature by van Soest, Benes, de Wit, and Vliegenthart (1996).

The radius of gyration distributions was also obtained by HPSEC-MALLS in water (i.e. in θ conditions). These distributions are very broad, because of a high dispersity (Fig. 1) and the radii of gyration of the major population of macromolecules are 77 nm and 180 nm for the extruded and the native potato starch respectively. Even if the starch macromolecules were depolymerized by extrusion, a small fraction of undamaged amylopectin remains (radius of gyration ≈190 nm).

The weight average radius of gyration $\overline{R_{Gw}R}$ of starch macromolecules after melt processing, calculated on the whole distribution of each samples, is about 100 nm. The weight-average radius of gyration ($\overline{R_{Gw}R}$) of the solubilized macromolecules in θ conditions corresponds to the radius of gyration in the melt and in the amorphous state (de Gennes, 1979). The average size of the macromolecules in the amorphous starch would then be: $2 \times \overline{R_{Gw}} \approx 200$ nm. Though no measurements could be made on the extruded starch containing clays, we will assume that the same approximated value applies for all bionanocomposites samples (see Section 4).

3.1.2. Distribution and dispersion state of clay nanoparticles

Fig. 6 shows typical images obtained in TEM observations for bionanocomposites containing 3%, 5% and 10% of clay (additional images for the same samples were previously reported by Coativy et al., 2014). For each concentration, clay particles were well distributed throughout the starch matrix. The biggest remaining clay aggregate size was close to 100 nm, while most of the tactoids were well disagglomerated and had a thickness smaller than 10 nm. The quality of the dispersion observed, with partially exfoliated structures, is similar to the only available results in literature concerning extruded bionanocomposites with starch, unmodified MMT and no other plasticizer than water (Dean, Yu, & Wu, 2007). Effectively, this simple system is actually quite different from the vast majority of the recently reviewed literature on starch-clay bionanocomposites (Vazquez, Cyras, Alvarez, & Moran, 2012) which generally deals with the reinforcement by clay (sometimes organomodified), of plasticized thermoplastic starch containing large amounts of glycerol and most of the time consisting of composite films obtained by casting from water.

Fig. 2 shows the corresponding X ray diffractograms: The diffractograms present two peaks associated to clay structure. The first peak is associated to the interlayer distance d_{001}, while the second peak is associated to atomic plane, within the clay layers. A detailed analysis of both peaks, including the evaluation of anisotropy as been provided in our earlier paper (Coativy et al., 2014). In particular, it was shown that the clay platelets are slightly oriented in the extrusion direction, whatever the clay content.

If we focus here on the first peak, we can see that position of its maximum and its width does not change with clay loading, indicating that both the interlayer distance and the average thickness of clay tactoïds are constant. The interlayer distance in the bionanocomposites is actually very close to the initial value observed for the clay, before melt mixing with starch.

The analysis of the peak width using the Scherrer law (Eq. (2)) allows us to estimate an average thickness of the tactoids equal to 6.8 nm corresponding on 4–5 layers per tactoids (Benetti et al., 2005; Coativy et al., 2014; Jaboyedoff et al., 1999).

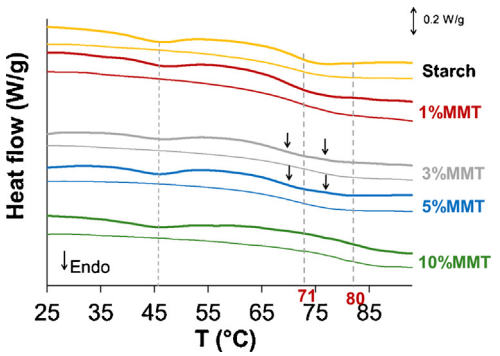

Fig. 3. Differential scanning calorimetry thermograms obtained for extruded starch and bionanocomposites (bold and thin lines correspond to the first and second heating ramps, respectively). The black arrows point out thermal events present in the glass transition region.

The intensity of the peak varies with clay content. In Fig. 2, we have plotted the intensity of the first peak vs clay loading, showing a linear increase with clay content, it suggests a constant exfoliation degree.

3.2. Calorimetric and thermomechanical behavior

The DSC thermograms and DMTA curves obtained on the extruded rods are presented in Figs. 3 and 4, respectively. The corresponding data are summarized in Table 1.

Before considering the results, it is important to point out that all analyzed samples had almost the same water content (13.7 ± 0.2%),

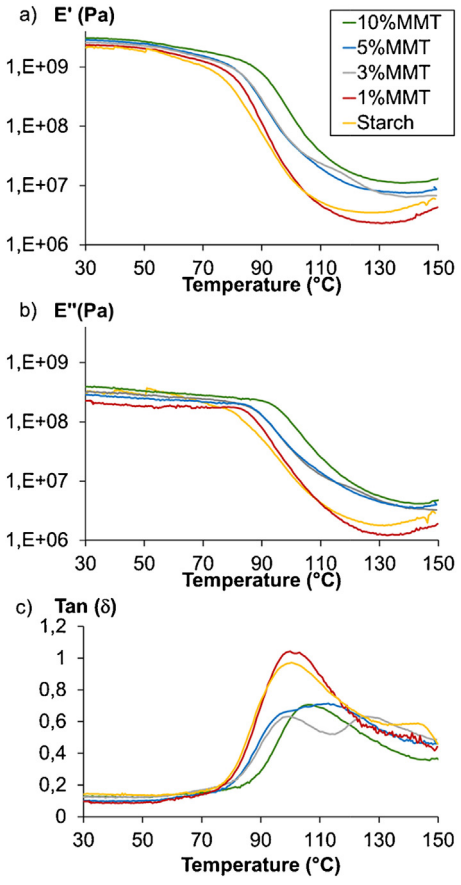

Fig. 4. DMTA curves obtained on extruded rods: storage modulus (a), loss modulus (b) and loss angle tangent (c).

which allows a detailed investigation of the influence of clay content on the relaxations of starch macromolecules. We assume that the presence of clay does not disturb the water distribution inside the matrix.

The DSC curves, presented in Fig. 3, show one physical aging endotherm between 40 and 50 °C, which disappears on the second heating (Borde, Bizot, Vigier, & Buleon, 2002). In the higher temperature region, during the first heating, glass transitions phenomena can be observed (Fig. 3 and Table 1). The starch reference, for the first and the second heating, shows only one typical glass transition (T_{g1} = 71 °C). As an opposition, during the first heating the nanocomposites containing 1%, 3% and 5% MMT show two events (highlighted by black arrows) in the glass transition. The first event is centered on 67 °C and the second appears about 10 °C above, at 77 °C. The second event is very weak and is not observed on the second temperature scan. Finally, the nanocomposite containing 10% MMT shows only one well defined glass transition in the first and the second scan at 80 °C, which is 9 °C higher than the T_g of the starch reference.

Fig. 4a shows the evolution of the storage modulus E' with temperature, while Fig. 4b and c respectively show the corresponding evolution of the loss modulus and of the tangent of the loss angle tan δ.

Below 70 °C approximately, all samples display a storage modulus E' in the GPa range, typical of the glassy state. Above 80 °C, the α mechanical relaxation associated to the glass transition of the starch matrix takes place, leading to a drop of the storage modulus until 110 °C. At 110 °C, in the rubbery state, the storage modulus ranges from 3 to 10 MPa, when clays content increases from 0 to 10%. For temperatures above 130 °C, the storage modulus starts to increase due to dehydration of the samples. Dehydration is particularly important for the pure starch sample, suggesting a fast water loss above 130 °C. In the case of the bionanocomposites, the increase of the storage modulus due to dehydration seems to occur at higher temperature. The average glassy and rubbery state values of E', reported in Table 1, are higher in presence of clay. The glassy modulus increases gradually with the clay loading, from 1.9 for unreinforced starch to 3.1 GPa for 10% of MMT. On the contrary, in the rubbery state, the storage modulus strongly increases between 1% and 3% clay loadings by 100%. Compared to the unreinforced starch, the elastic modulus is two times higher for the bionanocomposite containing 10% of MMT.

Besides, the loss modulus and tan(δ) curves, presented in Fig. 4b and c, show a more complex evolution of the thermomechanical behavior in presence of clay. While for the unreinforced starch sample and the bionanocomposite containing 1% of clay, a single peak ($T_{\alpha 1} \approx 99$ °C) is observed in the α relaxation temperature range (70–130 °C), two overlapped peaks are observed in the case of the bionanocomposites containing 3% and 5% of clay, suggesting a dynamic heterogeneity of the starch matrix, with two thermomechanical relaxations. This can be also observed on the loss modulus curves (Fig. 4b), but it appears more clearly on the tan δ curves (Fig. 4c).

According to the temperatures of the maximum of the tan δ peaks (T_α) reported in Table 1, the first relaxation takes place at the same temperature $T_{\alpha 1} \approx 100$ °C as the unreinforced starch, while the second relaxation associated to the additional peak seems to take place at a higher temperature which decreases with increasing clay content ($T_{\alpha 2}$ = 115–124 °C). The relative intensities of the two peaks show that the strength of this second relaxation increases between 3% and 5% clay loading. Finally, for a clay loading of 10%, a single relaxation peak is observed with a maximum at $T_{\alpha 1} \approx 107$ °C and smaller width than for the other compositions. Similar increase of T_α was obtained by Park and al. on starch-clay bionanocomposites plasticized with 15% glycerol (Park et al., 2002).

Table 1
Thermo-mechanical properties of the extruded rods (obtained by DSC and DMTA).

Sample	1st heating		2nd heating	Water (%)	E'_{glassy} (Gpa)	$T_{\alpha 1}$ (°C)	$T_{\alpha 2}$ (°C)	$E'_{rubbery}$ (Mpa)
	T (°C) 1st event	T (°C) 2nd event	T (°C)					
Starch	71 ± 2		71 ± 2	13.8 ± 0.2	1.9 ± 0.3	100 ± 3	–	3 ± 1
1%MMT	71		71	13.7	2.3	99	–	2
3%MMT	67 ± 2	77 ± 2	73 ± 2	13.8 ± 0.2	2.5 ± 0.2	98 ± 5	124 ± 5	7 ± 2
5%MMT	67	77	71	13.8	2.9	98	115	8
10%MMT	80		80	13.9	3.1 ± 0.1	107 ± 1	–	11 ± 2

If one compares the DSC and DMTA data, the α relaxation observed at $T_{\alpha 1} \approx 99$–$100\,^{\circ}C$ for all other samples except for 10% clay loading, is clearly linked to the (first) glass transition ($T_{g1} = 71\,^{\circ}C$) of unreinforced starch. For the sample containing 10% clay, we assume that the α relaxation observed at $T_{\alpha 1} \approx 107\,^{\circ}C$ can be associated with the glass transition observed at 80 °C, since the gap between T_g and T_α values remains the same as in the other samples. Only a 8 °C temperature shift takes place for both values.

As an opposition, for the samples containing 3% and 5% clay, it seems that the second event of the glass transition observed in DSC ($T_{g2} = 77\,^{\circ}C$, about 5 °C above T_{g1}) cannot easily be linked to the change observed with DMTA (about 20 °C).

3.3. Molecular mobility by NMR

In order to have a more local insight at the starch chains structure and how they are affected by the addition of clays, ^{13}C solid-state NMR experiments were performed on the following samples: 10% clay loading, 5% clay loading and the unreinforced starch reference sample. The spectra, not shown here but available as supporting information, show that at the NMR scale (chemical links conformations: a few Å), no structural differences exist between these three samples: the local structure of starch chains is not affected by the clay loading. However, by deconvoluting the spectra one can have access to parameters more relevant to our case. The spectra are fitted using Gaussian–Lorentzian partial components profiles, whose yield the lowest residuals. We use the works of Paris et al. on amorphous starch structure (Paris, Bizot, Emery, Buzare, Buleon, 1999; Paris, Bizot, Emery, Buzare, Buleon, 2001) as a reference. Fig. 5 presents the unreinforced starch CP-MAS spectrum (top) with the corresponding spectral decomposition (bottom), and labels each of the 9 peaks found. For each of these individual peaks, chemical shift (ppm), area (i.e. the relative importance of a specific peak), width (in ppm or Hz) and ratio of Gaussian over Lorentzian component were obtained. Of these four parameters the half-height width is of particular relevance for us because it is directly proportional to $1/T_2$, with T_2 the spin–spin relaxation time.

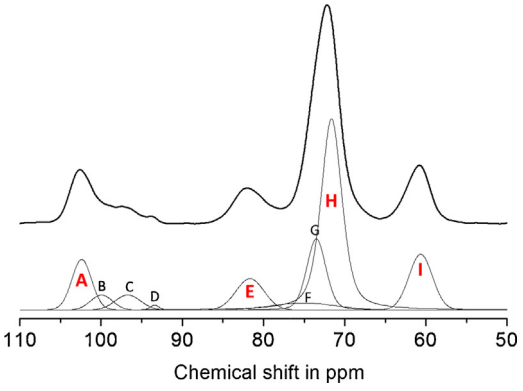

Fig. 5. ^{13}C NMR CP-MAS spectra of an extruded pure starch sample (top) with the corresponding decomposition in nine individual Gaussian–Lorentzian components (bottom). Peaks A, E, H and I (highlighted in red) are chosen to monitor the widening induced by clay loading. (For interpretation of the references to color in this legend, the reader is referred to the web version of the article.)

Table 2
Half height width of the deconvoluted NMR peaks for pure starch, and the difference from this reference for 5% clay and 10% clay samples, both in absolute (Hz) and relative values.

Peak ref.	Pure starch	Starch + 5% MMT	Starch + 10% MMT
A	0 (286.7 Hz)	+14.4 Hz/+5.0%	+43.1 Hz/+15.0%
E	0 (408.0 Hz)	+12.2 Hz/+3.0%	+34.6 Hz/+8.5%
H	0 (304.5 Hz)	+13.9 Hz/+4.6%	+48.3 Hz/+15.9%
I	0 (343.2 Hz)	+32.1 Hz/+9.4%	+36.8 Hz/+10.7%

The difference from the pure starch fitted half-height width for 4 peaks of each spectrum is reported in Table 2. These 4 peaks were chosen because they stand out more than the others and are thus more easily modeled and less subject to fitting errors. The width is found to be increasing with increasing clay loading, indicating a shorter T_2. From this result we can infer that adding clays to starch material hinders the chains movements, resulting in slower chain dynamics.

4. Discussion

DSC, DMTA and NMR results highlight a significant heterogeneity of macromolecular dynamics in the bionanocomposites. Whereas for low clay (1%MMT) content, no impact of the presence of clay was observed, a slowdown of segmental relaxation for the 10% MMT was evidenced by a 10 °C increase of T_g and T_α, and by an extension of the width of the NMR peaks. The intermediate concentrations, 3 and 5%MMT, present a more complex dynamic. Indeed, the presence of two overlapped α relaxation peaks and two thermal events in the glass transitions suggest the coexistence of two populations of macromolecules. As mentioned in the introduction, these phenomena have been observed in many polymer nanocomposites and can be inferred to the presence of an interphase and/or to the confinement of macromolecules between clays.

In order to better identify the involved phenomena, we propose to compare the size of the macromolecules ($2*\overline{R_{gw}}$) estimated by chromatography and the inter-particle distance (d) as a function of starch/clay ratio. Since no statistic TEM investigation was realized to determine the average interparticle distance, a predictive model based on dispersion state determined by X-ray diffraction will be used.

According to literature results obtained for fully exfoliated polyamide/clay nanocomposites characterized by detailed image analysis of TEM micrographs (Luo & Koo, 2008), the mean interparticle distance can be reasonably predicted by the following model (Luo & Koo, 2008), based on the stereological principle:

$$d = d_0 \times \frac{(w/\rho_{clay}) + ((1-w)/\rho_{matrix})}{w/\rho_{clay}} \quad (4)$$

where d_0 is the effective thickness of exfoliated clay platelets, equal to the initial basal spacing of clay tactoids before melt mixing with the polymer (it is assumed *that* $d_0 \ll d$); w is the mass fraction of

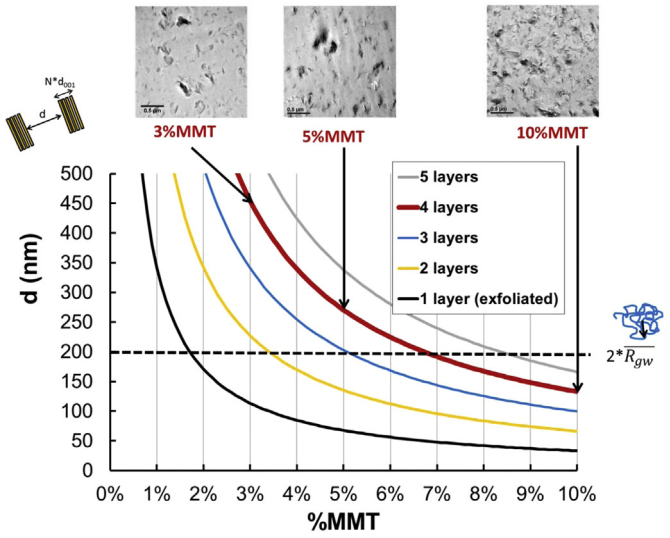

Fig. 6. Calculated theoretical inter-particle distance vs clay loading, depending on the number of stacked clay layers in each tactoid.

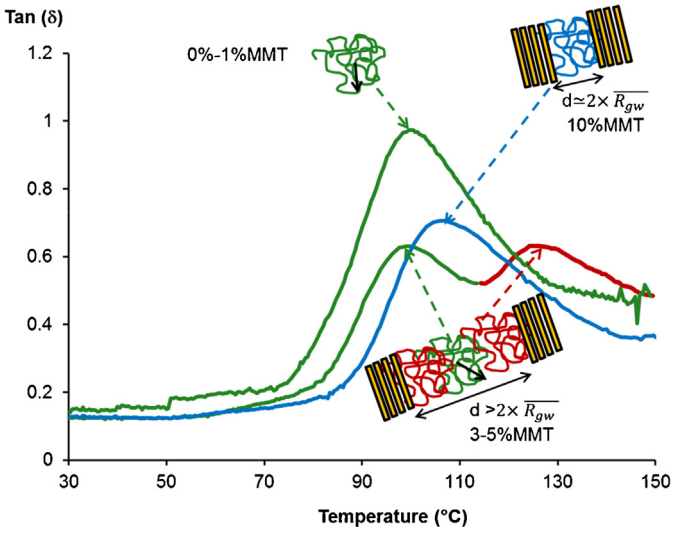

Fig. 7. Schematic view of the different types of interaction between starch and clay and related DMTA relaxations for unreinforced starch (green line), nanocomposites containing 3–5% (green and red line) and 10% clay (blue line). (For interpretation of the references to color in this legend, the reader is referred to the web version of the article.)

clay; and ρ_{clay} and ρ_{matrix} are the densities of the clay and the polymer matrix, respectively.

In our case, the results obtained with X-ray diffraction and TEM showed that the bionanocomposites contain mainly tactoids with an average thickness of 6.8 nm, thus containing between 4 and 5 stacked layers, but also thinner particles, including fully exfoliated platelets, and some remaining aggregates (according to TEM observation). Thus, a large distribution of particle thickness is observed.

Therefore, following the approach described by Luo and Koo (2008), we have applied the stereological principle in that slightly more complex case, taking also into account the presence of water. The equation that we obtain allows evaluating the inter-particle distance for particles of different average particle thicknesses:

$$d = n \times d_{001} \times \frac{(W_{clay}/\rho_{clay}) + (W_{starch}/\rho_{starch}) + (W_{water}/\rho_{water})}{W_{clay}/\rho_{clay}} \quad (5)$$

where n is the number of layers in the particle, d_{001} = 1.6 nm is the average interlayer distance in native clay; w_{clay}, w_{starch} and w_{water} are the mass fractions of the three components in the bionanocomposite; and ρ_{clay} = 2.6, ρ_{starch} = 1.5 and ρ_{water} = 1, their densities. Note that just as Eq. (4) of Luo and Koo, the validity of Eq. (5) relies on the fact that the calculated average interparticle distances are large compared to the thickness of the particles.

Fig. 6 shows the calculated theoretical mean inter-particle distance as a function of the clay loading (d.b.) using Eq. (5) for particles containing between 1 (fully exfoliated platelets) and 5 stacked clay layers, respectively. The inter-particle distance range represented is limited to 500 nm for the sake of clarity. As expected, for a given clay loading the predicted inter-particle distance increases with the number of stacked clay layers per tactoid. While for a given number of clay per tactoid, the inter-particle distance decreases when the clay content increase. We also observe that for a concentration smaller than 2% MMT, even if the clay are fully exfoliated, the calculated average inter particle distance remains higher than the average macromolecular size $2\overline{*R_{gw}}$. On the contrary, for a concentration higher than 8%MMT the average macromolecular size $2\overline{*R_{gw}}$ is smaller than the inter particle distance for each dispersion state, confinement can occur (Dionne Rahmi & Picu, 2005). For intermediate concentration, confinement is really sensitive to dispersion state, in the present case (4–5 layers per tactoid) the confinement effect is not predominant. The calculated distances are coherent with distance range observed by TEM.

Taking into account these observations, we propose an interpretation based on the existence of three macromolecular populations with different mobility which are described in the following lines and summarize in the form of a scheme in Fig. 7. The first population (green), which has a bulk behavior with T_{g1} and $T_{\alpha 1}$ values close to those observed for unreinforced starch, is present in all bionanocomposites, except that containing 10% clay. It would correspond to the segmental relaxation of "bulk" macromolecules that are not in contact with clay nanoparticles ($d \gg 2\overline{*R_{gw}}$).

The second population (blue), with T_{g1} and $T_{\alpha 1}$ shifted about 10 °C toward higher temperatures compared to unreinforced starch, is observed for the bionanocomposite containing 10% clay by both DSC and DMTA and could be eventually present for a small fraction in the 3%MMT and 5%MMT nanocomposites for the biggest macromolecules and/or for exfoliated clays. It would correspond to the macromolecules that are confined between clay nanoparticles ($d < 2\overline{*R_{gw}}$) having a slowed down segmental relaxation, NMR supports this assumption. Such a phenomenon has already been observed in other nanocomposites for clay loadings lower than 10%MMT, while for higher the segmental mobility was fully suppressed (Fotadiou et al., 2013; Vaia et al., 1997).

The third population (red) could be present for intermediate clay loadings (3–5%), and would come from starch-clay attractive interactions. In the present case, the second thermal event observed during the glass transition by DSC, is consistent with the presence of an interphase coming from a strong affinity between starch and montmorillonites which are both hydrophilic (Rittigstein & Torkelson, 2006; Rittigstein et al., 2007). Besides, particles can act as "crosslinkers" by adsorbing monomers into their surface leading to the suppression of the terminal flow relaxation (diffusion/reptation) or the increase of the associated time-temperature (Kalfus & Jancar, 2007; Robertson & Rackaitis, 2011). The presence of the second peak observed on DMTA curves could come from this retardation. In future studies, it would be interesting to try to model the influence of such an immobilized phase on the reinforcement of starch using existing approaches such as the one described by Chazeau, Cavaillé, Canova, Dendeviel, and Boutherin (1999) in the case of cellulose nanowhiskers reinforced PVC.

Finally, the absence of the second peak and the thinness of the observed alpha relaxation peak for the 10%MMT sample suggest the suppression of the terminal relaxation in the observed time

temperature window for the most highly confined macromolecules and could be eventually present at higher temperature.

5. Conclusion

In the present work, the dynamic of starch macromolecules in bionanocomposites containing natural montmorillonite (MMT) was studied by DSC, NMR, DMTA. It pointed out a dynamic heterogeneity in presence of clays. The evaluated macromolecular size and the modeled interparticle distance suggest a confinement effect responsible for the segmental dynamic and flow relaxation retardation for high clay loadings (10%MMT). While for intermediate clay loading (3–5% MMT), a starch interphase seems to be observed, having a slowed down dynamic on finite spatial dimension and coexisting with a bulk polymer.

These results suggest that, since the ratio between macromolecular size and interparticle distance ($2 * \overline{R_{gw}}/d$) seems to be determinant for the confinement, the widespread goal to control the dispersion state of the nanoparticle into the reinforced nanocomposites should go with a preservation of the macromolecules size: soft process should be preferred to incorporate clays into the matrix.

Acknowledgements

The authors would like to gratefully thank the Région des Pays de la Loire and the Department INSIS of CNRS for the Ph.D. grant attributed to Gildas Coativy. The authors also thank Marion De Carvalho, Sophie Guilois, Bruno Pontoire, Loïc Foucat and Nicolas Gautier for their excellent technical assistance.

References

Bansal, A., Yang, H. C., Li, C. Z., Cho, K. W., Benicewicz, B. C., Kumar, S. K., et al. (2005). Quantitative equivalence between polymer nanocomposites and thin polymer films. *Nature Materials*, *4*, 693–698.

Benetti, E. M., Causin, V., Marega, C., Marigo, A., Ferrara, G., Ferraro, A., et al. (2005). Morphological and structural characterization of polypropylene based nanocomposites. *Polymer*, *46*, 8275–8285.

Borde, B., Bizot, H., Vigier, G., & Buleon, A. (2002). Calorimetric analysis of the structural relaxation in partially hydrated amorphous polysaccharides. II. Phenomenological study of physical ageing. *Carbohydrate Polymers*, *48*, 111–123.

Chazeau, L., Cavaillé, J. Y., Canova, G., Dendeviel, R., & Boutherin, B. (1999). Viscoelastic properties of plasticized PVC reinforced with cellulose whiskers. *Journal of Applied Polymer Science*, *71*, 1797–1808.

Coativy, G., Gautier, N., Pontoire, B., Buléon, A., Lourdin, D., & Leroy, E. (2014). Shape memory starch-clay bionanocomposites. *Carbohydrate Polymers*, http://dx.doi.org/10.1016/j.carbpol.2013.12.024

Dean, K., Yu, L., & Wu, D. Y. (2007). Preparation and characterization of melt-extruded thermoplastic starch/clay nanocomposites. *Composite Science and Technology*, *67*, 413–421.

de Gennes, P. G. (1979). *Scaling concepts in polymer physics*. Ithaca, N.Y.: Cornell University Press.

Dionne, P. J. O., & Rahmi Picu, R. C. (2005). Structure and dynamics of polyethylene nanocomposites. *Macromolecules*, *38*, 9351–9358.

Fotadiou, S. K., Chrissopoulou, C., Karatasos, K., Tanis, I., Tragoudaras, D., Frick, B., et al. (2013). Structure and dynamics of hyperbranched polymer/layered silicate nanocomposites. *Macromolecules*, *46*, 2842–2855.

Fragiadakis, D., Bokobza, L., & Pissis, P. (2011). Dynamics near the filler surface in natural rubber-silica nanocomposites. *Polymer*, *52*, 3175–3182.

Giannelis, E. P. (1998). Polymer-layered silicate nanocomposites: Synthesis, properties and applications. *Applied Organometallic Chemistry*, *12*, 675–680.

Jaboyedoff, M., Kubler, B., & Thelin, P. H. (1999). An empirical Scherrer equation for weakly swelling mixed-layer minerals, especially illite–smectite. *Clay Minerals*, *34*, 601–617.

Jancar, J., Douglas, J. F., Starr, F. W., Kumar, S. K., Cassagnau, P., Lesser, A. J., et al. (2010). Current issues in research on structure–property relationships in polymer nanocomposites. *Polymer*, *51*, 3321–3343.

Huang, W. L., Bassett, W. A., & Wu, T. C. (1994). Dehydration and hydration of montmorillonite at elevated-temperatures and pressures monitored using synchrotron-radiation. *American Mineralogist*, *79*(7–8), 683–691.

Kalfus, J., & Jancar, J. (2007). Relaxation processes in PVAc-HA nanocomposites. *Journal of Polymer Science Part B: Polymer Physics*, *45*, 1380–1388.

Kalfus, J., & Jancar, J. (2008). Reinforcing mechanisms in amorphous polymer nanocomposites. *Composites Science and Technology*, *68*, 3444–3447.

Luo, Z. P., & Koo, J. H. (2008). Quantification of the layer dispersion degree in polymer layered silicate nanocomposites by transmission electron microscopy. *Polymer*, *49*, 1841–1852.

Paris, M., Bizot, H., Emery, J., Buzare, J. Y., & Buleon, A. (1999). Crystallinity and structuring role of water in native and recrystallized starches by C-13 CP-MAS NMR spectroscopy: 1. Spectral decomposition. *Carbohydrate Polymers*, *39*, 327–339.

Paris, M., Bizot, H., Emery, J., Buzare, J. Y., & Buleon, A. (2001). NMR local range investigations in amorphous starchy substrates: I. Structural heterogeneity probed by C-13 CP-MAS NMR. *International Journal of Biological Macromolecules*, *29*, 127–136.

Park, H. M., Li, X. C., Jin, C. Z., Park, C. Y., Cho, W. J., & Ha, C. S. (2002). Preparation and properties of biodegradable thermoplastic starch/clay hybrids. *Macromolecular Materials and Engineering*, *287*, 553–558.

Rittigstein, P. T., & Torkelson, J. M. (2006). Polymer–nanoparticle interfacial interactions in polymer nanocomposites: confinement effects on glass transition temperature and suppression of physical aging. *Journal of Polymer Science Part B: Polymer Physics*, *44*, 2935–2943.

Rittigstein, P., Priestley, R. D., Broadbelt, L. J., & Torkelson, J. M. (2007). Model polymer nanocomposites provide an understanding of confinement effects in real nanocomposites. *Nature Materials*, *6*, 278–282.

Robertson, C. G., & Rackaitis, M. (2011). Further consideration of viscoelastic two glass transition behavior of nanoparticle-filled polymers. *Macromolecules*, *44*, 1177–1181.

Roger, P., & Colonna, P. (1992). The influence of chain length on the hydrodynamic behavior of amylose. *Carbohydrate Research*, *227*, 73–83.

Rolland-Sabate, A., Guilois, S., Jaillais, B., & Colonna, P. (2011). Molecular size and mass distributions of native starches using complementary separation methods: Asymmetrical flow field flow fractionation (A4F) and hydrodynamic and size exclusion chromatography (HDC-SEC). *Analytical and Bioanalytical Chemistry*, *399*, 1493–1505.

Sankri, A., Arhaliass, A., Dez, I., Gaumont, A. C., Grohens, Y., Lourdin, D., et al. (2010). Thermoplastic starch plasticized by an ionic liquid. *Carbohydrate Polymers*, *82*, 256–263.

Vaia, R. A., Sauer, B. B., Tse, O. K., & Giannelis, E. P. (1997). Relaxations of confined chains in polymer nanocomposites: Glass transition properties of poly(ethylene oxide) intercalated in montmorillonite. *Journal of Polymer Science Part B: Polymer Physics*, *35*, 59–67.

Vaia, R. A., & Giannelis, E. P. (1997). Lattice model of polymer melt intercalation in organically-modified layered silicates. *Macromolecules*, *30*, 7990–7999.

Vaia, R. A., & Wagner, H. D. (2004). Framework for nanocomposites. *Materials Today*, *7*(11), 32–37.

van Soest, J. J. G., Benes, K., de Wit, D., & Vliegenthart, J. F. G. (1996). Influence of starch molecular mass on the properties of extruded thermoplastic starch. *Polymer*, *37*, 3543–3552.

Vazquez, A., Cyras, V. P., Alvarez, V., & Moran, J. (2012). In L. Avérous, & E. Pollet (Eds.), *Environmental silicate nano-biocomposites* (pp. 287–321). London: Springer.

Wu, A. C., Witt, T., & Gilbert, R. G. (2013). Characterization methods for starch-based materials: state of the art and perspectives. *Australian Journal of Chemistry*, *66*(12), 1550–1563.